Phase space geometry of chaotic reactive scattering: Gateways, windings, and halos

H. Wadi and L. Wiesenfeld
Laboratoire de Spectrométrie Physique, Université Joseph-Fourier Grenoble, Boîte Postale 87, 38402 Saint-Martin-d'Hères Cedex, France
(Received 7 May 1996)

We present a renewed geometrical approach to classical reactive scattering. We treat here a linear triatomic indirect reaction. Geometry in phase space is presented by means of a careful analysis of the asymptotic motion and its consequences on finite-distance properties. It allows us to define a gateway to the reaction and probability densities on the surface of section. Because of chaos, the gateway is surrounded by windings, whose existence is proved. Windings are grouped in halos, on which statistical repartition of reactants is assumed. Halos allow us to treat the whole chaotic scattering in a simple and meaningful way. By measuring areas, we are able to calculate the reaction probability in a simple but realistic model. This computation agrees with averaging over trajectories. [S1063-651X(97)09601-3]

PACS number(s): 05.45.+b, 34.10.+x, 82.20.Fd

I. INTRODUCTION

There has appeared recently a renewed interest in chaotic scattering as a tool to deal with reactive scattering in chemical physics. The coming of age of classical scattering theory (for a review, see [1]) has prompted a number of authors, including ourselves, to try to apply the concepts of transient chaos to the understanding of individual, simple chemical events. One of the goals of all those studies is to try to calculate and possibly to understand the outcome of an elementary chemical reaction, knowing that the reactants are statistically distributed in a well defined manner prior to the reaction [2,3]. In this way, microscopic dynamics would be related to chemical kinetics. Very simply here, we would like to devise a simple geometrical way to calculate *and* to depict the statistical outcome of a simple triatomic reactive collision $A+BC \leftrightarrow ABC \leftrightarrow A+BC$, where A,B,C are symbols for single atoms. Even more simplified, we shall deal here, like in another paper [4], exclusively with the collinear, symmetric reaction $A+BA' \leftrightarrow ABA' \leftrightarrow AB+A'$ and try to calculate its reaction rate at a defined energy.

Thus we wish in this paper to present a classical mechanics approach to reactive scattering through *geometry and probability flows in phase space*. We shall limit ourselves here to the first steps in this direction, within the framework of a rudimentary model. This model — two-dimensional configuration space, Morse potentials between atoms— shows, nevertheless, the essential features we are looking for: (i) an asymptotic free motion of the fragments, which represents the states before reaction, and (ii) chaotic dynamics inside the interaction region, since chaos is the rule rather than the exception in any general scattering process. Through a geometrical analysis of transport in phase space we shall tend to replace averages over trajectories by measures of surface areas and their intersections. We hope that such a geometrical view will open the way to a qualitative understanding of the phenomena at hand, for it offers a global visualization of the reaction process. This approach relies heavily on two approximations: first, the Born-Openheimer approximation, with one electronic level completely decoupled from all others throughout the reactive event and second, a classical approximation to the nuclear motion within this single potential sheet. These approximations, even if somewhat restrictive, have to be employed in order to pinpoint the role of chaos in reactive scattering. The type of analysis presented here has been partly inspired by analogous ideas that have been developed in bound systems. Transport in phase space through turnstiles has been known for some time now [5,6] and applied in the context of microscopic physics (classical and quantum) by Bohigas and coworkers [7]. Their successful extensions of transport in phase space into the quantum regime is also an encouraging prospect.

A. Chaos theory

From the dynamical point of view, much progress has been made these past years in the theory of unbound Hamiltonian chaos. Chaos has long been suspected to play an important role in the dynamics of the molecular collisions [8] and by now, chaotic scattering theory is well established, in both its classical [1] and quantum [9] versions. Simple models such as the three-disk system have been completely analyzed; they demonstrated the existence of transient chaos for Hamiltonian dynamics [10]. Chaotic scattering has the distinctive feature that the finite distance dynamics with all its intricacies projects itself towards infinity through the Hamiltonian flow. Conversely, the asymptotic conditions are faithfully projected into the interacting region. As a consequence, we have access to the properties of the chaotic motion thanks to suitable observables and we should be able to gain profit of the nowadays well-known structures that exist in scattering chaos.

All previous attempts that dealt with chaos together with reactive scattering, including our own, concentrated on the long-time behavior of chaotic dynamics. They focused on the singularities of the various deflection functions that connect incoming to outgoing asymptotic regions of the scattering event. These singularities arise from the image through the Hamiltonian flow of the invariant set that exists at finite distance. They consist in the periodic and quasiperiodic orbits embedded in the overall flow (for an image of such a set, see [4] and Fig. 9 therein). It is clear that finding such an invari-

ant set amounts to exploring the dynamics at the infinite time limit, in order to distinguish the invariant orbits with respect to the very long ones. Knowing the multifractal properties of this invariant set allows one to compute the asymptotic properties of the scattering chaos. Especially of interest are the average Lyapunov exponent and the escape rate. This approach *did not*, however, allow us to calculate the average value of observables of chemical interest and, in particular, the reaction rate.

B. Chemical physics

Without emphasis on Hamiltonian chaos, reaction dynamics has been the subject of a very large number of theoretical works that have concentrated on one aspect or another, at different levels of sophistication. In order to obtain the variations of the differential or integral cross sections, one resorts most often to a time-independent quantum formalism or to classical trajectory calculations. Even if they are usually not limited by the number of dynamical states or channels, quantum calculations become very difficult as soon as the number of degrees of freedom increases [11]. Nevertheless, a very good knowledge of the scattering event may be gained from the behavior of the different vibrational energy levels, which contain all the information, at least in the Born-Oppenheimer limit [12]. In classical formalisms, one computes trajectories and averages over suitable statistical ensembles (microcanonical or canonical). Access to the various differential cross sections is easy. However, because of their usual limitation to configuration (coordinate) space, it is difficult to correlate the results with the shape of potential surfaces or chemical and dynamical variables. Also, because of the blind averaging process, one cannot determine the influence and importance of a given physical parameter in the actual value of an observable.

Some steps in the direction of geometrical analysis, which prompted us to do the sudy presented here, had been undertaken in the pioneering works by Pollak, Child, and Pechukas, extending over many years [13]. They showed clearly the crucial importance of the periodic orbits and especially of the periodic orbit dividing surfaces (PODS). Without the present-day knowledge of scattering chaos they analyzed in depth the flow in configuration as well as in phase space and discovered the windings phenomena, without any proof [14].

Somewhat later, several other authors began studies of the phase-space geometry of simple chemical reactions [15–18]. The relevant concepts of transport in phase space were used in those papers, in particular for unimolecular reactions and the $H+H_2$ reaction. These concepts were applied in order to criticize and improve transition state theory (TST) and to calculate reaction rates. Indeed, many of the studies dealt with the classical transition state problem. A clear image of the transition state would be a section in phase space that clearly distinguishes the flux containing only products of the reaction. It was recognized earlier that such a definition has to be carefully scrutinized because of the occurrence of chaos and ever reentering trajectories. Still, the theory of transport in phase space, together with the notion of turnstiles, proved to be the right tools to extend TST for general situations. In order to fully compare these approaches with ours, we shall finish this discussion in Sec. VII.

Also, by determining the Lyapunov exponent of primary periodic orbits at finite distance and by computing their unstable manifolds, it became possible to associate resonances with those orbits. Therefrom, many classical and semiclassical analyses were proposed. Recently, semiclassical chaotic scattering has been examined in some detail (see [19], where many earlier references are cited). These authors concentrate on the periodic orbit analysis in order to reconstruct the whole scattering picture and to recover a semiclassical image by summation in a trace formula. An analysis of finite-distance properties of the chaotic motion in the double Morse potential, based on the stable and unstable manifolds of the various periodic orbits, was also proposed by Berblinger and Schlier [20]. Also in a preceeding paper [4], studied in depth were the finite-distance properties of the scattering chaos: periodic orbits, invariant set, hierarchy of orbits, as well as the influence of those properties on global aspects of chaos. Symbolic dynamics was proposed in [4] as well as in [21]. It summarizes all the properties of the finite-distance chaos. Some other recent papers also analyzed a model chemical reaction in the spirit of chaotic scattering [22,23]. A description of the scattering process is given and also some parts of the underlying hierarchy are described.

The paper is organized as follows. Section II describes the model we use as well as the relevant Hamiltonians. Then we show in Sec. III that the reaction has to proceed through special parts of the phase space, called gateways. We then organize the chaos into windings (Sec. IV) and halos (Sec. V), on which we define measures and probabilities before computing an actual model reaction rate and concluding. In order to anchor our approach in firm ground, we found it nececessary to adopt in several subsections rather mathematical language. The interested reader may thus go into all technical details of our demonstrations. However, the reader interested mostly in the geometrical and computational results may easily skip the relevant sections and avoid the somewhat cumbersome notations we introduced. The actual demonstrations of lemmas and a theorem are postponed to Appendices, so that the reader may more easily follow the physical arguments. A preliminary and shortened version of this paper is published elsewhere [24].

II. MODEL

A. Classical, collinear reactive scattering

The reaction model we shall use must be sufficiently simple in order not to be blurred with unnecessary considerations, yet general enough so that the conclusions of the present analysis are easily transposable to more accurate and relevant models of chemical reactions. The first and most important limitation that we impose is the restriction to a single internuclear potential sheet. The whole subsequent theory in its present form is thus adiabatic. Even if there exist now many classical and semiclassical ways to overcome this restriction and to treat properly the nonadiabatic transitions [25], we cannot include this complexity in a first description.

The second limitation is that we make use of a classical image of the dynamics and not a quantum one. This approximation, largely used in the literature, relies on the heavy masses of the nuclei. It is valid as long as the de Broglie

FIG. 1. Collinear configuration of the three atoms in collision. r_{l1} and r_{l2} are the two local coordinates.

wavelength does not vary too rapidly $d\lambda_{\mathrm{dB}}/\lambda_{\mathrm{dB}} \ll 1$. Equivalently, if S is a characteristic action of the motion, we have $S/\hbar \gg 1$. We explicitly neglect such effects as tunneling, which are known to be non-negligible for light reactantlike hydrogen or deuterium. Also, quantization of rotation and vibration is, of course, not included.

The third limitation that we are forced into for the moment is that we deal only with a collinear, symmetric reaction (Fig. 1). The two degrees of freedom are r_{l1}, r_{l2}, the internuclear distances with a fixed center of mass. The two diatoms AB and BA' interact exclusively with identical Morse potentials. If this two-dimensional restriction is somewhat limiting, and may be thought to be less credible from a chemical physics point of view, it is still indispensable for a visual approach to phase-space analysis. Actually, the vast majority of studies of dynamics in phase space is done with the following dimensional scheme: configuration space 2D, phase space $2\times 2 = 4$D, constant energy shell $4-1=3$D, and Poincaré section $3-1=2$D. A well chosen section is a faithful image of the dynamics. If the section is 2D, it can be easily printed and visualized. The main advantage of the model we used, besides its simplicity and generality, is that it has been studied many times and in great detail and the previous analyses are compatible.

B. Hamiltonians

We use the following model of the symmetric collinear reaction. Let A, B, A' be the three atoms and let the relative coordinates (or local coordinates) be $r_{l1} = |r_A - r_B|$ and $r_{l2} = |r_{A'} - r_B|$ (Fig. 1). By eliminating center-of-mass motion, we obtain the Hamiltonian with kinetic coupling

$$\mathcal{H} = \frac{p_{l1}^2}{2m_{AB}} + \frac{p_{l2}^2}{2m_{AB}} - \frac{1}{m_B} p_{l1} p_{l2} + V_1(r_{l1}) + V_2(r_{l2}), \quad (1)$$

with m_{AB} the reduced mass $[m_{IJ} = m_I m_J/(m_I + m_J)]$. In order to restore the image of a pure potential motion, one changes from kinetic to potential couplings [26,27]. In the simple symmetric triatomic configuration, the kinetic coupling can be removed by introducing two new kinematic parameters

$$\cos\varphi = \frac{1}{1 + m_B/m_A}, \quad (2)$$

$$m = \frac{m_A(m_A + m_B)}{2m_A + m_B}. \quad (3)$$

Oblique coordinates are then defined as

$$r_{o1} = r_{l1} + r_{l2}\cos\varphi, \quad (4)$$

$$r_{o2} = r_{l2}\sin\varphi \quad (5)$$

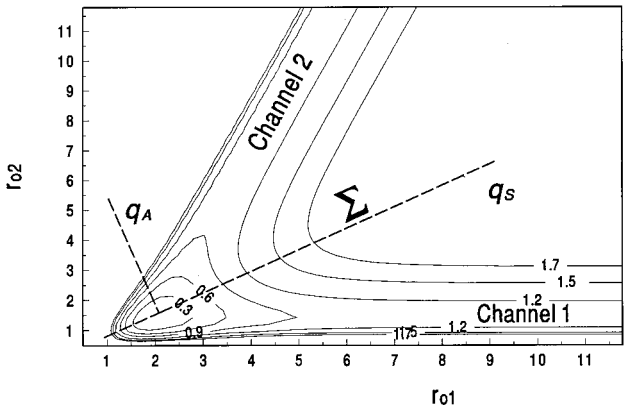

FIG. 2. Morse potential in oblique reduced coordinates. The projection of the Σ section is shown together with the two reaction channels. All quantities plotted here and in all subsequent figures are dimensionless.

and the conjugate momenta p_{o1} and p_{o2} follow easily. The Hamiltonian in oblique coordinates, with potential coupling, becomes

$$\mathcal{H} = \frac{1}{2m}(p_{o1}^2 + p_{o2}^2) + V_1(r_{o1}, r_{o2}) + V_2(r_{o2}). \quad (6)$$

The Morse potential is written as

$$V_{\mathrm{Morse}}(r) = D(1 - e^{-a(r-R_e)})^2. \quad (7)$$

In this configuration, one may resort to the following reduced coordinates, denoted by their tildes:

$$\tilde{r} = ar, \quad (8)$$

$$\tilde{p} = p/\sqrt{m_{AB}D}, \quad (9)$$

$$\tilde{t} = a\sqrt{D/m_{AB}}\,t, \quad (10)$$

$$\tilde{\mathcal{H}} = \mathcal{H}/D. \quad (11)$$

Please note the disappearance of a factor of 2 with respect to [4]. Since in the following we will use *reduced oblique coordinates* only, obtained from r_{o1} and r_{o2}, we apply the simple notation q_1, q_2 and p_1, p_2 for these new coordinates and their conjugate momenta, respectively. In these variables, the reduced Hamiltonian for the ABA case is

$$\tilde{\mathcal{H}} = \frac{\sin^2\varphi}{2}(p_1^2 + p_2^2) + \{1 - \exp[-(q_1 - q_2\cot\varphi - \tilde{R}_e)]\}^2 + \{1 - \exp[-(q_2/\sin\varphi - \tilde{R}_e)]\}^2. \quad (12)$$

Symmetric and antisymmetric coordinates are easily defined as (Fig. 2)

$$q_S = (r_{o1} + r_{o2})/\sqrt{2}, \quad (13)$$

$$q_A = (r_{o1} - r_{o2})/\sqrt{2}. \quad (14)$$

Only two parameters remain to determine the dynamics, namely, the reduced energy $\tilde{E}$ and the mass ratio $\cos\varphi$. In all

subsequent figures, we set $m_A/m_B=0.5$ and the reduced energy $\widetilde{E}=1.4$. These values do not qualitatively affect the pictures.

Let us describe the peculiarities of the potential form used so that we can point out the limitations and the ways to overcome them.

(i) There is no finite distance threshold. Also the $AB\cdots A'$ vibration periodic orbit is set to infinity *and* is marginally stable, a zero Lyapunov exponent.

(ii) The asymptotic behavior of the Morse potential is very peculiar; this has been clearly indicated in [4]. However, multipolar long-distance potentials between ground-state atoms and molecules are attractive and behave like $r^{-n}, n\geqslant 6$, which is very similar, for practical purposes, to the Morse potential. The infinitely distant periodic orbit is marignally stable since $n>2$.

(iii) For $1<\widetilde{E}<2$ Morse potentials support *two* finite-distance periodic orbits of a period of the order of one (in reduced units), namely, the antisymmetric, stable $q_S=0$ orbit and the symmetric, unstable $q_A=0$ orbit. There exists, thus, in the middle of the chaotic saddle a stable island whose dynamics is disconnected with asymptotic motion. Fortunately, this island is surrounded by a strong, highly unstable 1:3 resonance that limits the influence of the stable islands and the cantori. It has been observed in [4] that only high in the hierarchy of orbits are the sticky tori observable. We shall completely neglect this complication.

C. Asymptotic motion

Let us limit ourselves to one of the channels $r_{l1}\gg r_{l2}, r_e$, that is, $q_1\gg\widetilde{R}_e$ [28]. In reduced, oblique coordinates, the Hamiltonian (12), we have approximately

$$\mathcal{H}=\mathcal{H}_1+\mathcal{H}_2+1, \tag{15}$$

where

$$\mathcal{H}_1=\frac{\sin^2\varphi p_1^2}{2}, \tag{16}$$

$$\mathcal{H}_2=\frac{\sin^2\varphi p_2^2}{2}+V(q_2). \tag{17}$$

One sees readily that the Hamiltonian (16) corresponds to the free translation energy $\widetilde{E}_t$ while the other, Hamiltonian (17), energy $\widetilde{E}_v$ describes free diatomic vibration. These energies are quasiadditive. The vibrational fraction is readily expressed in this picture as $f_v=\widetilde{E}_v/\widetilde{E}$.

III. GATEWAYS

A. Entrance and exit gates

In this section, we describe the geometrical pathways through which the reaction has to proceed in the phase space. Let us choose a Poincaré surface of section Σ that is dividing. Such a surface is crossed at least once by any trajectory, but for the symmetric periodic orbit. This dividing surface is here the $q_A=0$ surface (see Sec. II and Fig. 2). On that surface there exists well defined domains that act as entrance and exit gates to and from the interaction region and connect

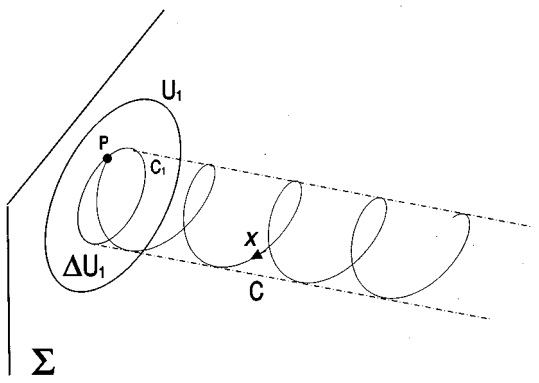

FIG. 3. Scheme of a trajectory **x** winding on the cylinder C. All trajectories belonging to C differ only by a phase. The intersection of **x** and the Σ plane is the point P. It lies on a closed convex curve C_1, inside U_1, with the unstable manifold of the periodic orbit at infinity. ΔU_1 is the interior of U_1.

it to the asymptotic regions at infinity. We shall call both the entrance and the exit the ''gateways'' of the reaction.

In Sec. II C we defined a first asymptotic part of the scattering trajectory. It corresponds to a vibrating AB oscillator and an A' atom whose motion is nearly decoupled. In the potential coupling image (Hamiltonian in oblique coordinates), with a fixed center of mass, the energy $\widetilde{E}$ is divided into vibrational $\widetilde{E}_v$ (the AB motion) and translational $\widetilde{E}_t$ (incoming A' atom). In phase space, the representative point has two nearly independent motions: the first one at constant momentum, describing the translational motion, and the second one, a closed circularlike curve, describing the oscillatory motion. Their combination yields a helical trajectory. For a fixed value of $\widetilde{E}_v$, all the helices differ only by a phase and assemble to form a surface having in phase space the topology of a cylindrical surface (see Fig. 3). Varying continuously the value of $\widetilde{E}_v$ between 0 and $\widetilde{E}$ amounts to varying continuously the diameter of the cylinder, thus covering the whole three-dimensional manifold of all trajectories at a given energy. Let us call this cylindrical volume C.

Since the surface of section Σ is dividing, any trajectory belonging to the above-described cylinder C must cross Σ at least once. That is, the set of all first intersections between Σ and C has a disklike topology. We call ΔU_1 the disk and U_1 its border. The border U_1, being the trace of the widest possible cylinder, belongs to orbits having as much vibrational energy as possible. These orbits belong to the unstable manifold of the infinitely distant periodic orbit; see [4]. One may thus identify this unstable manifold with U_1 on Σ.

The potential surface being symmetric with respect to Σ, there corresponds to any trajectory a twin one, symmetric with respect to Σ. Both cross Σ at the same point (q_S,p_S), but with an opposite sign of p_A (Fig. 4). Also, inverting the direction of any trajectory is equivalent to changing the sign of the momenta and thus transforming a (q_S,p_S) point on Σ into a $(q_S,-p_S)$ point. We deduce that (i) ΔU_1 is the set of all first intersections of scattering trajectories coming from *either channel*, and (ii) by making the transformation $\hat{T}(q_S,p_S)\doteq(q_S,-p_S)$, the ΔU_1 set is transformed into $\Delta S_1=\hat{T}(\Delta U_1)$. ΔS_1 is the set of all *last* intersections between the Σ plane and the trajectories before they depart

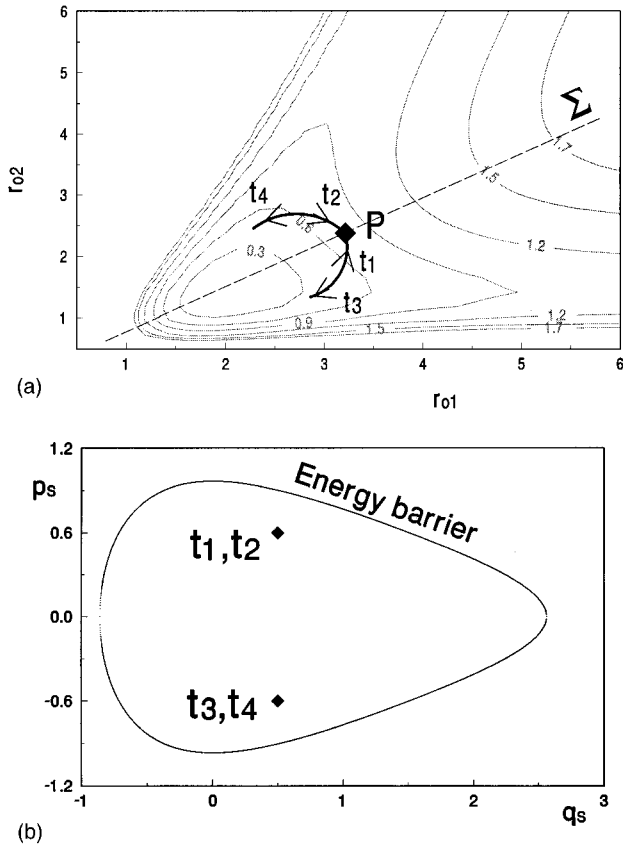

FIG. 4. (a) Four trajectories represented by one point on Σ in configuration space. (b) Same trajectories in the Σ section; the two points are related by time inversion.

definitely to infinity, in either channel. In analogy to ΔU_1, the border of $\Delta S_1, S_1$ belongs to the stable manifold of the infinitely distant periodic orbits. Let us stress again that (i) to each point of ΔU_1 there correspond two twin trajectories, coming from each channel, and (ii) to each point of ΔS_1 there correspond two twin trajectories, aiming at each channel.

The set

$$\Delta G = \Delta U_1 \cup \Delta S_1 \tag{18}$$

will be called the *gateway* of the reaction. It is shown in Fig. 5.

We denote by $\hat{M}$ the mapping associated with the Poincaré section Σ. By definition, $\Delta U_n = \hat{M}(\Delta U_{n-1})$ and $U_n = \hat{M}(U_{n-1})$. The $\Delta U_n, n = 1,2, \ldots,$ tile the whole region of Σ allowed by energy. If we denote by $\hat{M}^{-1}$ the inverse map of $\hat{M}$ and we define $\Delta S_n = \hat{M}^{-1} \Delta S_{n-1}$, another tiling of the Σ section by the set of the $\Delta S_n, n = 1,2, \ldots,$ may be found.

Let us discuss the ΔU_n tiles. First, they cover the whole region, except for a set of measure zero, the invariant set of the chaotic scattering [29]; see [4] for details. Second, let us suppose there exists a point $P \in \Delta U_m \cap \Delta U_n$, $m < n$. Then, let us take its mth inverse image, implying $\hat{M}^{-m}(P) \notin \Sigma$ for $\hat{M}^{-m}(\Delta U_m)$ not defined and $\hat{M}^{-m}(P) \in \Sigma$ for $\hat{M}^{-m}(\Delta U_n)$, $m < n$, defined. So there is no P for any *finite* value of m, n.

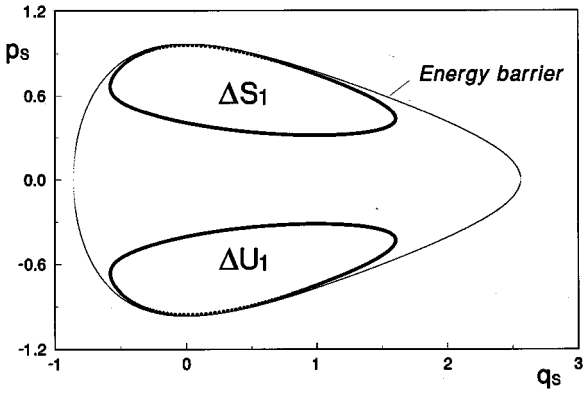

FIG. 5. Gateway to the reaction: ΔU_1, entrance gate; ΔS_1, exit gate.

As a conclusion to this subsection, we organized the allowed region in Σ into a disjoint set of successive mappings of the entrance and exit gates. In the asymptotic region, the entrance dynamical states are very well defined; they are represented in the model by the vibrational energy probabilities. On the surface of section at infinity $\mathcal{S}^\infty$, the microcanonical ensemble will be described by a density probability ρ^∞. The Cartan-Liouville theorem allows us to define probability densities in phase space, especially on the $\mathcal{S}^\infty$ section ($r_{o1} \to \infty$). This probability density, *which is conserved in the Hamiltonian flow*, is transported towards the interaction region. Then, by the definition of the entrance gate ΔU_1, through its one-to-one correspondence with $\mathcal{S}^\infty$, we project the density probability of the exterior world inside the reaction dynamics (see Fig. 6). The reaction proceeds by successive mappings to progressively cover ΔS_1 by the images of ΔU_1. This will define on ΔS_1 a probability density after the reaction. Similarly, for the same reasons, the reaction dynamics is projected from ΔS_1 to the products of the reaction, again at infinity, in the outside world. Therefore, associating probabilities with possible microcanonical dynamical states is equivalent to associating a probability density function with the entrance and exit gates $\Delta G = \Delta U_1 \cup \Delta S_1$.

It is clear that the gateway may remind the reader of the turnstiles defined by Wiggins or others [6] as a tool for analyzing transport in phase space. There are, however, differences. One is that the lobes composing the turnstile are bordered by both stable and unstable manifolds, while here the

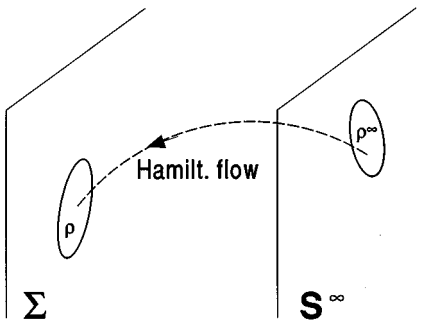

FIG. 6. Hamiltonian flow projects a surface from infinity to the Σ section.

perspective is such that some lobes are purely stable (or unstable) and some are mixed. Also, the definition of the U_n, S_n sets is unique, in contrast to the relative character of the ordering of lobes. This comes about from the existence of unbound, separable motion that puts a clear limit to the unbound chaos, in opposition to phase-space motion in the presence of bound chaos. A more general and full description of the phase space at hand is deferred to a future work. Now, we have to define measures on the sets and find the way these measures follow the mappings.

B. Measure on the gates

The dynamics of the reactive scattering being Hamiltonian, it is straightforward to define an invariant measure in phase space, thanks to the Cartan-Liouville theorem. Let us denote by $\mu(\Delta U_n)$ a measure of ΔU_n. As we have chosen Σ to be spanned by two conjugate coordinates (q_S, p_S) (i.e., $\{q_S, p_S\}=1$), we may identify the measure and area

$$\mu(\Delta U_n)=\int_{\Delta U_n} dq_S dp_S . \tag{19}$$

As stated in the Introduction, the scattering system is open. This means that the total number of trajectories present in the interaction region diminishes after each Poincaré mapping $\hat{M}$. The measure of the successive images ΔU_n must show this decrease. Indeed, as any scattering trajectory leaves the Σ surface through ΔS_1, we have the relation

$$\mu(\Delta U_n)=\mu(\Delta U_{n-1})-\mu(\Delta U_{n-1}\cap \Delta S_1). \tag{20}$$

We may also inquire about the fate of a sufficiently small element of surface $\delta S=\delta q_S \delta p_S$ belonging to the entrance gate ΔU_1. After a certain number of successive iterations of $\hat{M}$, it will be projected into the exit gate ΔS_1. In the mapping process, its measure will be conserved, so that $\delta S(\text{entrance})=\delta S(\text{exit})$ for the set of invariant orbits is of measure zero. This conservation of measure has often been underlined in different contexts of chaotic Hamiltonian dynamics [1].

Being equipped with a measure, it is now possible to associate a probability density function $\rho(q_S, p_S)$ with each point $(q_S, p_S)\in \Delta U_1$, as well as an element of probability $dP_S=\rho dq_S dp_S$. We associate with an area $\mathcal{A}$ in ΔU_1 the probability

$$P(\mathcal{A})=\int_{\mathcal{A}} dP_S=\int_{\mathcal{A}} \rho(q_S, p_S) dq_S dp_S . \tag{21}$$

Through the mappings $\hat{M}$, this probability density function will be transferred from the entrance gate ΔU_1 to the exit gate ΔS_1. Let us look at the conservation rule of $P(\mathcal{A})$. If $\mathcal{A}_n$ is the nth image of an area through the mapping $\hat{M}$ and $dP_n=\rho_n dS_n$ an element of probability defined on it, one has

$$\rho_n \overset{\hat{M}}{\Rightarrow} \rho_{n+1},$$

$$dP_n=\rho_n dS_n \overset{\hat{M}}{\Rightarrow} dP_{n+1}=\rho_{n+1} dS_{n+1}.$$

As trajectories are conserved for sufficiently small areas, $dP_n=dP_{n+1}$ and by the Cartan-Liouville theorem, $dS_n=dS_{n+1}$. Thus

$$\rho_n(q_S, p_S)=\rho_{n+1}(\hat{M}(q_S, p_S)). \tag{22}$$

This process eventually transforms $\rho(q_S, p_S)$ into $\rho'(q'_S, p'_S)$, with $(q'_S, p'_S)\in \Delta S_1$. In summary, knowing the transformation

$$\rho \overset{R}{\mapsto} \rho' \tag{23}$$

is the same as knowing how the reaction proceeds inside the interaction region between the gateways (Fig. 5). The transformation R contains all the geometrical information about the reaction mechanism. We changed the problem from a statistical analysis of trajectories to a problem of topology and measure of surfaces: What are the surfaces of intersection between the successive $\Delta U_n, n=1,2,\ldots$, and the exit ΔS_1? Let us remark here that the R transformation may be simple for nonchaotic processes or exceedingly complicated if the motion is chaotic.

Finally, but most important, we also need to evaluate the mean values of the physical observables, such as reaction probability and vibrational energy. If $\hat{\Omega}$ is any (classical) observable, it will take on ΔU_1 the value $\Omega(q_S, p_S)$, thanks to the Hamiltonian flow from $\mathcal{S}^{\infty}$ towards Σ. The set of points satisfying $\Omega \leqslant \Omega(q_S, p_S) \leqslant \Omega + d\Omega$ will be an element of surface belonging to ΔU_1. By spanning the Ω value, ΔU_1 will be charted by the different values the $\hat{\Omega}$ observable takes on it. Similarly, by transforming (q_S, p_S) into $(q_S, -p_S)$ we obtain the corresponding chart on ΔS_1, the exit gate. The whole gateway is labeled by the values of the $\Omega(q_S, p_S)$ function, for reactants and products. The mean values at the entrance and exit are easily calculated:

$$\langle \hat{\Omega} \rangle_{\text{in}}=\int_{\Delta U_1} \Omega(q_S, p_S)\rho(q_S, p_S) dq_S dp_S , \tag{24}$$

$$\langle \hat{\Omega} \rangle_{\text{out}}=\int_{\Delta S_1} \Omega(q_S, p_S)\rho'(q_S, p_S) dq_S dp_S . \tag{25}$$

Knowing the charts on the gateway and the reaction transformation $\rho \overset{R}{\mapsto} \rho'$ allows one to calculate the mapping

$$\langle \hat{\Omega} \rangle_{\text{in}} \overset{R}{\mapsto} \langle \hat{\Omega} \rangle_{\text{out}} .$$

It is thus possible to know to which kind of statistical distribution the reactive scattering event heads.

IV. WINDINGS

This section aims at showing the consequences of the winding theorem on the topology of the ΔU_n surfaces, or in other words, on the reaction dynamics. We shall thus first have some definitions, state the theorem, outline its demon-

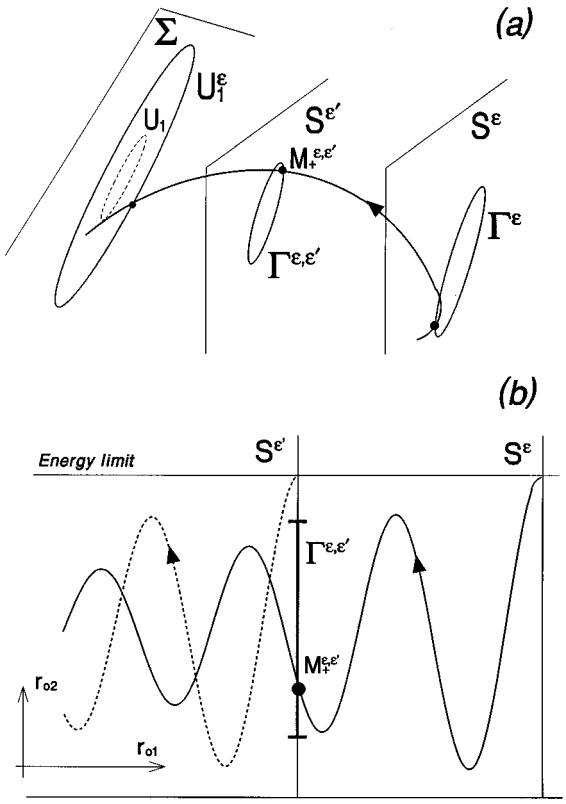

FIG. 7. Various sections and curves associated with a trajectory ending in $\mathcal{S}^\varepsilon$ (see the text for details): (a) in ''perspective'' and (b) in configuration space. The decrease of amplitude of the vibrational motion is grossly exagerated.

stration, and then return to the consequences on the shapes of the successive ΔU_n. The complete demonstration is shown in the Appendixes and the less mathematatically oriented reader may go from here to Fig. 8 and then to Sec. IV C.

A. Definitions and notations

For all that follows, we suppose that $r_{oi} \gg r_{oj}$. Let us also recall that $V_{\text{Morse}} \to 1$ for $r_{oi} \to \infty$.

Let us denote by r_{oi}^ε the value of r_{oi} that verifies (for $r_{oi}^\varepsilon > R_e$)

$$V_{\text{Morse}}(r_{oi}^\varepsilon) = 1 - \varepsilon \Rightarrow \lim_{\varepsilon \to 0} r_{oi}^\varepsilon = R_e - \ln \varepsilon / 2.$$

Let us now consider trajectories whose translational kinetic energy E_t goes to zero for the section $\mathcal{S}^\varepsilon \equiv r_{oi} = r_{oi}^\varepsilon$ (let us recall that $\mathcal{S}^{\varepsilon=0} \equiv \mathcal{S}^\infty$). Section $\mathcal{S}^\varepsilon$ is spanned by conjugate coordinates r_{oj}, p_{oj}. The Hamiltonian reads

$$H = \frac{p_{oj}^2}{2m} + V_1(r_{oi}^\varepsilon, r_{oj}) + V_2(r_{oj}).$$

This relation defines on $\mathcal{S}^\varepsilon$ a closed curve, which we denote Γ^ε; see Fig. 7.

Since the V_{Morse} potential is strictly increasing for $r_{oi} > R_e$, any trajectory going through Γ^ε has to cross the Σ Poincaré section at least once. We denote by U_1^ε the intersection with Σ of all trajectories coming from Γ^ε, and $\Gamma^{\varepsilon,\varepsilon'}$ the set of all intersections with another section $\mathcal{S}^{\varepsilon'}$ ($\varepsilon' \geqslant \varepsilon$). We identify Γ^ε with $\Gamma^{\varepsilon,\varepsilon}$ (Fig. 7).

We see thus that the $\varepsilon \geqslant 0$ parameter is used to label the furthest section a given trajectory may reach. A trajectory that reaches infinity with zero kinetic translational energy is characterized by $\varepsilon = 0$. Now, let us describe a given section $\mathcal{S}^{\varepsilon'}$, with $\varepsilon' > \varepsilon$. The $\mathcal{S}^\varepsilon$ section is thus *further* away from the interaction region than the $\mathcal{S}^{\varepsilon'}$ section. It is easy to convince oneself that different curves $\Gamma^{\varepsilon,\varepsilon'}$, $\varepsilon \neq \varepsilon'$, may not cross. Now, a trajectory that grazed the Γ^ε curve loses some vibrational energy in the course of its progression from $\mathcal{S}^\varepsilon$ towards $\mathcal{S}^{\varepsilon'}$ (Fig. 7), even if this loss is exponentially small [30]. Since the $\mathcal{S}^{\varepsilon'}$ section displays the vibrational coordinates—remember that vibration and translation are nearly separable in the asymptotic region—the $\Gamma^{\varepsilon,\varepsilon'}$ is surrounded by the $\Gamma^{\varepsilon'}$ closed curve. The argument may be repeated for any triplet $\varepsilon' > \varepsilon_1 > \varepsilon_2$: The $\Gamma^{\varepsilon'}$ curve encircles the $\Gamma^{\varepsilon_1,\varepsilon'}$ curve, which itself encircles the $\Gamma^{\varepsilon_2,\varepsilon'}$ curve. The Hamiltonian flow transports this structure to the Σ section without disturbing it, as long as the nearest section $\mathcal{S}^{\varepsilon_0}$ still belongs to the asymptotic region.

Knowing further that $\lim_{\varepsilon \to 0} U_1^\varepsilon = U_1$, we find that the U_1^ε curves encircle U_1 for $\varepsilon > 0$ and U_1^ε encircles $U_1^{\varepsilon'}$ if $\varepsilon > \varepsilon'$. We have thus surrounded U_1 by a foliation of U_1^ε, with ε uniformly increasing with distance to U_1.

If we now apply in Σ the time-reversal transformation $\hat{T}(q_S, p_S) = (q_S, -p_S)$, we obtain from the family U_1^ε a new family S_1^ε, encircling the stable manifold S_1: $\hat{T}(U_1^\varepsilon) = S_1^\varepsilon$. Then, U_1^ε is the set of first interactions with Σ of trajectories issued from the $\mathcal{S}^\varepsilon$ section at zero kinetic translational energy and S_1^ε is the set of trajectories obtained from U_1^ε by inverting the sign of momenta. These are thus trajectories whose translational kinetic energy goes to zero on $\mathcal{S}^\varepsilon$. As before, we have, for any value of ε, $\hat{M}(U_n^\varepsilon) = U_{n+1}^\varepsilon$ and $\hat{M}^{-1}(S_n^\varepsilon) = S_{n+1}^\varepsilon$ As a closure relation, we have also $\hat{M}(S_1^\varepsilon) = U_1^\varepsilon$.

B. Winding theorem

We may now state precisely the theorem (Fig. 8).

If (i) I belongs to S_1, (ii) P belongs to $S_1^{\varepsilon_0}$, (iii) $\overline{PI}$ is a curve of finite length, and (iv) by going on $\overline{PI}$, from P to I, we define a bijection between the successive points on $\overline{PI}$ and the S_1^ε curves, with ε diminishing continuously from ε_0 to 0, then $\hat{M}(\overline{PI})$ is a spiral winding infinitely around U_1.

For the ease of the reader, the demonstration of the theorem is dealt with in Appendix C. The theorem is essentially a consequence of the definitions of S_1. S_1 is the border between trajectories that will return and cross Σ once more and trajectories that have just crossed Σ for the last time before definitely going away. So the nearer a point from $\overline{PI}$ is to S_1, the farther away the trajectory it defines will go into the asymptotic region and the nearer to U_1 it will again cross Σ. By continuity arguments and by an asymptotic analysis in

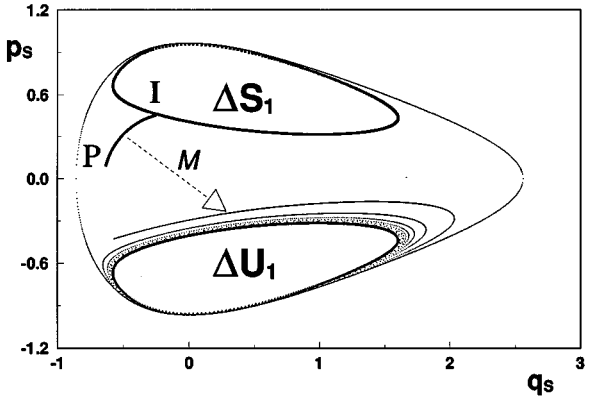

FIG. 8. Winding theorem. By the Poincaré mapping, the segment $\overline{PI}$ is mapped onto the spiral wound around ΔU_1.

phase, one can show the infinite spiral shape of the image of $\overline{PI}$.

C. Windings

In this section we describe the consequences of the winding theorem (WT) on the topology of the successive ΔU_n surfaces. Here we shall be very specific in our example: two coupled identical Morse potentials, mass ratio 1:2:1, and reduced energy $\widetilde{E}=1.4$; see Sec. II B.

In Fig. 9(a) the gateways ΔU_1 and ΔS_1 are represented together with the limiting curve $H=\widetilde{E}$. The entrance and exit gateways do not cross each other, so that at that particular energy and mass ratio, no trajectory crosses Σ only once. $\Delta U_2=\hat{M}(\Delta U_1)$ is also represented in the same figure. We see that ΔU_2 crosses S_1, so that $\Delta U_2 \cap \Delta S_1 \neq \emptyset$. Some trajectories go to infinity after having crossed Σ twice. Next, ΔU_1, ΔS_1, and ΔU_3 are represented in Fig. 9(b). ΔU_3 crosses ΔS_1. Some trajectories go to infinity after three crossings; these are the simplest reactive trajectories. We see that ΔU_3 is qualitatively different from $\Delta U_1, \Delta U_2$. It winds around ΔU_1 an infinite number of times, as a consequence of the crossing of U_2 and S_1: $\Delta U_3 \mathsf{W}_{\infty 1}(\Delta U_1)$. Next we see $\Delta U4$ in Fig. 9(c). We see that the following are true:

$$\Delta U_3 \text{ crosses } \Delta S_1 \overset{\text{WT}}{\Rightarrow} \Delta U_4 \mathsf{W}_{\infty 1}(\Delta U_1),$$

$$\Delta U_3 \mathsf{W}_{\infty 1}(\Delta U_1) \overset{\hat{M}}{\Rightarrow} \Delta U_4 \mathsf{W}_{\infty 1}(\Delta U_2).$$

For ΔU_5, something new appears again [see Fig. 9(d)]. Since $\Delta U_4 \mathsf{W}_{\infty 1}(\Delta U_2)$, the intersection of U_4 and S_1 is made of an infinity of disjoint bands, thinner and thinner as one nears the limit point $U_2 \cap S_1$ [see Fig. 9(c)]. The image of each of these bands is a winding of ΔU_5 around ΔU_1. In this way

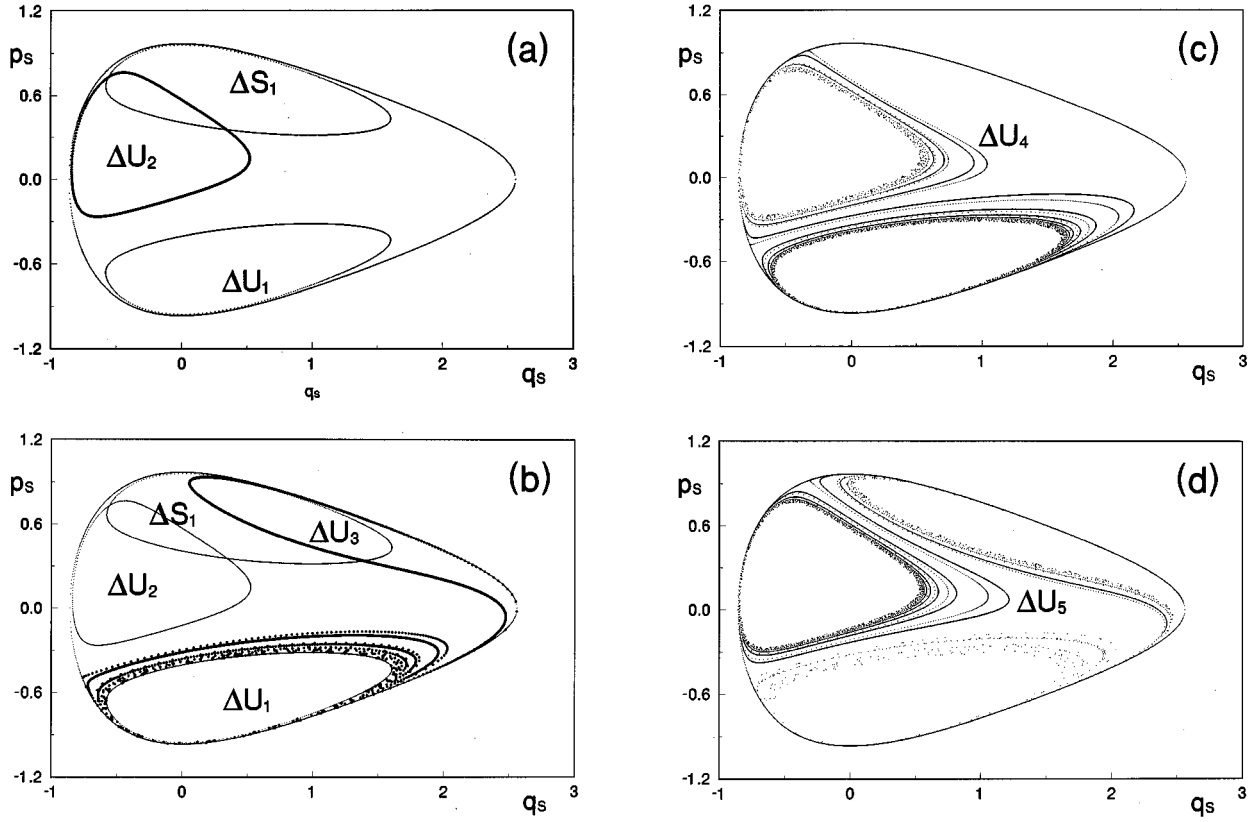

FIG. 9. Exit gateway ΔS_1 and the various mappings of ΔU_1. (a) The first map of ΔU_1, ΔU_2, retains a regular shape (finite perimeter). (b) The second mapping ΔU_3 winds an infinite number of times ΔU_1. (c) The third mapping ΔU_4 winds an infinite number of times ΔU_1 and ΔU_2. (d) The fourth mapping ΔU_5 winds an infinite number of times ΔU_3 and ΔU_2 and a double infinite number of times ΔU_1 (see the text).

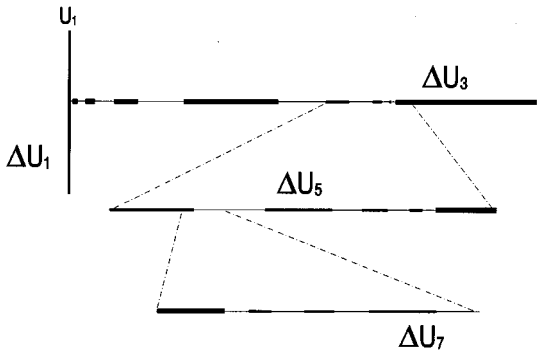

FIG. 10. Beginning of one hierarchy of discontinuities near U_1. One shows the odd series ΔU_7 which winds ΔU_5, which winds ΔU_3, which winds ΔU_1. Another series is generated by ΔU_4.

ΔU_5 winds around the winding of ΔU_3, i.e., $\Delta U_5 \mathsf{W}_{\infty 1}(\Delta U_3)$ and $\Delta U_5 \mathsf{W}_{\infty 2}(\Delta U_1)$. In summary,

$$\Delta U_4 \mathsf{W}_{\infty 1}(\Delta U_1) \overset{\hat{M}}{\Rightarrow} \Delta U_5 \mathsf{W}_{\infty 1}(\Delta U_2),$$

$$\left.\begin{matrix} \Delta U_4 \mathsf{W}_{\infty 1}(\Delta U_2) \\ \Delta U_2 \text{ crosses} \Delta S_1 \end{matrix}\right\} \overset{WT}{\Rightarrow} \left\{\begin{matrix} \Delta U_5 \mathsf{W}_{\infty 2}(\Delta U_1) \\ \Delta U_5 \mathsf{W}_{\infty 1}(\Delta U_3). \end{matrix}\right.$$

The ensemble of ΔU_n, $n=3,\ldots,\infty$, winds around ΔU_1 an infinite number of times, in a hierarchic self-similar way, as explained in Fig. 10. One may say that the analysis presented thus far concentrates on the trajectories in the asymptotic regions and their fate inside the interaction region. This analysis may be seen as complementary to the periodic orbit analysis and the multifractal aspects of the chaotic scattering described earlier; see [4] or many other earlier references on general chaotic scattering [10].

V. HALOS

In Sec. III we defined in the Poincare section Σ two particular zones that we called the gateways of the chemical reaction. We could define an entrance gate ΔU_1 and an exit gate ΔS_1. On both gates a probability density function was defined: $\rho(q_S,p_S)$ and $\rho'(q'_S,p'_S)$, respectively. The chemical reaction proceeds from $\rho(q_S,p_S)$ towards $\rho'(q'_S,p'_S)$.

Now, we have to answer simple questions about an isolated reaction: What is the overall reaction probability P_R and what is the mean value $\langle\hat{\Omega}\rangle$ of an observable $\hat{\Omega}$? Answering these problems amounts to knowing how ΔS_1 is covered by the successive images ΔU_n of ΔU_1. In particular, the set of reactive trajectories $\mathcal{R}$ is given by

$$\mathcal{R} = \bigcup_{k=1,2,\ldots} (\Delta U_{2k-1} \cap \Delta S_1), \tag{26}$$

as a reactive trajectory crosses the Σ section an *odd* number of times before leaving. We could measure $\mathcal{R}$ directly in a picture of Σ if the reaction were not chaotic, that is, in the absence of windings. To see that this task is impossible, it is sufficient to consider the set of windings around ΔU_1; see Fig. 9. The complexity of the covering of ΔS_1 by the successive ΔU_n precludes any direct measurement. Yet the total surface covered by the windings is far from negligible. In other words, windings compel us to speak in probabilistic terms in those regions where they are present. We shall determine the probability of encountering an odd or even winding, coming from any part of ΔU_1. This leads us to the concept of *halos*, whose purpose is to separate windings from the rest of the flux, thus dividing the covering of ΔS_1 into a regular and a probabilistic part: the ΔU_n surrounded by its halo dU_n.

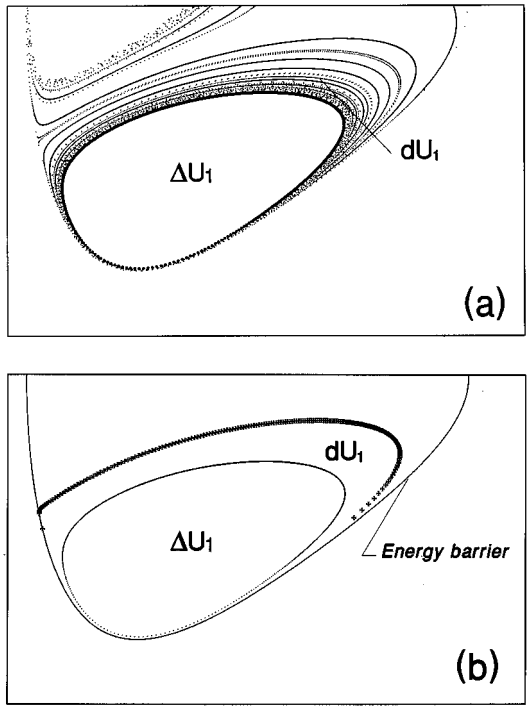

FIG. 11. (a) Windings surrounding ΔU_1 that form dU_1. (b) Halo dU_1.

A. Definition

Our aim is to properly delimit zones where the windings are located. The windings, which we defined in Sec. IV, come from trajectories whose translational energies go to zero far inside one of the channels. We introduce thus a critical distance $r_i^c = R^c, i=1,2$, with

$$V_{\text{Morse}}(r_i^c) = 1 - \varepsilon^c. \tag{27}$$

We call dU_1 the halo of ΔU_1; it is the set of the first intersection with Σ of all trajectories that begin with zero kinetic energy at a distance further from the equilibrium point than R^c. The set of all trajectories originating from the R^c section will exactly cross Σ on a closed line we call $U_1^{\varepsilon^c}$, which surrounds the unstable manifold U_1. The halo dU_1 is the region between the two curves U_1 and $U_1^{\varepsilon^c}$; see Fig. 11. Through the transformation $\hat{T}$, we define the halo dS_1 of ΔS_1 as the region between the S_1 and $S_1^{\varepsilon^c}$. Using the Poincaré map $\hat{M}$, one has

$$\hat{M}(S_1^{\varepsilon}) = U_1^{\varepsilon}, \quad \varepsilon \in (0,\varepsilon^c], \tag{28}$$

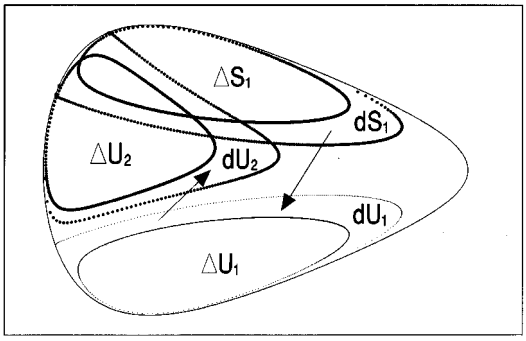

FIG. 12. Different Poincaré mappings, indicated by arrows, between dU_1, dU_2 and dS_1.

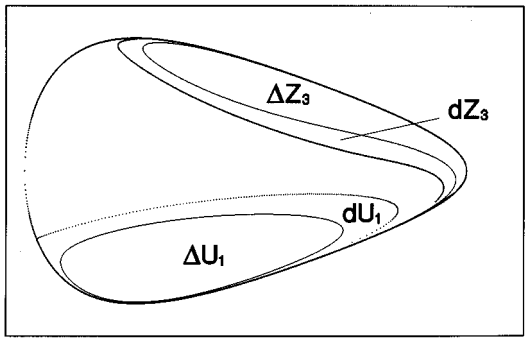

FIG. 13. Regular zone ΔZ_3 with its halo dZ_3, coming from the ensemble ΔU_3 [compare with Fig. 9(b)].

so that

$$\hat{M}(dS_1)=dU_1. \tag{29}$$

By taking successive images, we define $U_n^{\varepsilon^c}=\hat{M}(U_{n-1}^{\varepsilon^c})$, $n=2,3,\ldots$. Similarly, the region between U_n and $U_n^{\varepsilon^c}$ defines the halo of ΔU_n, denoted dU_n.

B. Pseudogateways

Let us consider the two sets $\mathcal{H}U_2=(\Delta U_2\cup dU_2)$ (the set *and* its halo) and $\mathcal{H}S_1=(\Delta S_1\cup dS_1)$; see Fig. 12. We know that any trajectory whose representative point lies inside ΔS_1 has no image, for the trajectory heads towards infinity after this last crossing. Therefore, the set $\mathcal{H}U_2\cap\Delta S_1$ has no image in Σ. On the other side, the images of the set $\mathcal{H}U_2\cap dS_1$ belong to the halo of ΔU_1, namely, dU_1: the outgoing translational energy of these trajectories goes to zero in either channel at a distance larger than R^c, so that they will again cross Σ, but inside the halo of ΔU_1. But these trajectories are already present in the halo dU_2. In order not to count them twice, we have to admit that

$$\hat{M}[\mathcal{H}U_2\cap dS_1] \tag{30}$$

is not defined. We may conclude that we have to admit here that the whole intersection of sets and halos $\mathcal{H}U_2\cap\mathcal{H}S_1$ has no image, similar to $\Delta U_2\cap\Delta S_1$ having strictly no image. In this sense, the union $\mathcal{H}G=\mathcal{H}U_1\cup\mathcal{H}S_1$ plays a role similar to the gateway $\Delta G=\Delta U_1\cup\Delta S_1$. Therefore, we call $\mathcal{H}G$ the *pseudogateway* of the reaction.

Let us now try to divide a given set into regular and irregular parts. ΔU_n is thus divided into a regular part ΔZ_n and a part that winds around some other set $\Delta U_n-\Delta Z_n$, thus being contained is some halo dU_m. We have the definitions (see Fig. 13)

$$Z_n=\hat{M}[U_{n-1}-(U_{n-1}\cap\mathcal{H}S_1)], \tag{31}$$

$$Z_n^{\varepsilon^c}=\hat{M}[U_{n-1}^{\varepsilon^c}-(U_{n-1}^{\varepsilon^c}\cap\mathcal{H}S_1)]. \tag{32}$$

We also define, in a coherent way,

$$Z_1=U_1, \tag{33}$$

$$Z_1^{\varepsilon^c}=U_1^{\varepsilon^c}. \tag{34}$$

As before, ΔZ_n is the interior of the Z_n curve, while dZ_n is its halo, between Z_n and $Z_n^{\varepsilon^c}$, and $\mathcal{H}Z_n=\Delta Z_n\cup dZ_n$.

We shall now see the exit gate ΔS_1 as being covered by elements of the different ΔZ_n and dZ_n. The former ones, $\Delta Z_n\cap\Delta S_1$ are the *regular* zones in the exit gate; they do not show windings, and numerical evalution of their measure is possible. On the contrary, the sets of the form $dZ_n\cap\Delta S_1$ contain all windings, by construction. They constitute the probabilistic zones of the exit gate. Inside an intersection $dZ_n\cap\Delta S_1$ all that is hoped for is to compute the measurement of a definite part coming from a subset of the entrance gate.

C. Probability densities

The reactive trajectories are those that cross Σ an odd number of times. Therefore, for the intersections $\Delta Z_n\cap\Delta S_1$, the probability of being reactive is 0 or 1, n being even or odd, respectively. For the probabilistic zone $dZ_n\cap\Delta S_1$, let us denote by P_n the probability of finding inside a reactive trajectory. We shall make the further hypothesis that the probability density associated with P_n is constant over the whole dZ_n surface. This amounts to supposing that all windings are uniformly distributed inside dZ_n.

Now, taking into account that any point of dZ_n is the image of a point in dZ_{n-1} and taking this relation back to $dZ_1\equiv dU_1$, we are led to

$$P_n=\begin{cases}P_1 & \text{for odd } n\\ 1-P_1 & \text{for even } n.\end{cases} \tag{35}$$

It is enough to calculate P_1 to obtain any P_n probability. In order to calculate P_1, let us begin with the following remark. The odd (even) windings of the intersections $\mathcal{H}Z_n\cap dS_1$ yield the even (odd) windings of dZ_1. This may be seen by forming the set $\hat{M}(\mathcal{H}Z_n\cap dS_1)$. From this remark, we obtain the following two relations on the measures:

$$P_1\mu(dZ_1)=\sum_{n\geqslant 1}\mu(\Delta Z_{2n}\cap dS_1)$$

$$+\sum_{n\geqslant 1}(1-P_n)\mu(dZ_n\cap dS_1) \tag{36}$$

and

$$(1-P_1)\mu(dZ_1)=\sum_{n\geqslant 1}\mu(\Delta Z_{2n-1}\cap dS_1)+\sum_{n\geqslant 1}P_n\mu(dZ_n\cap dS_1). \quad (37)$$

Summing Eqs. (36) and (37) we get

$$\mu(dZ_1)=\sum_{n\geqslant 1}\mu(\Delta Z_n\cap dS_1)+\sum_{n\geqslant 1}\mu(dZ_n\cap dS_1). \quad (38)$$

Using the relations for P_n [Eqs. (35)], relation (36) may be written

$$P_1\mu(dZ_1)=\sum_{n\geqslant 1}\mu(\Delta Z_{2n}\cap dS_1)+P_1\sum_{n\geqslant 1}\mu(dZ_{2n}\cap dS_1)+(1-P_1)\sum_{n\geqslant 1}\mu(dZ_{2n-1}\cap dS_1). \quad (39)$$

This leads to

$$P_1=\frac{\sum_{n\geqslant 1}\{\mu(\Delta Z_{2n}\cap dS_1)+\mu(dZ_{2n-1}\cap dS_1)\}}{\mu(dZ_1)+\sum_{n\geqslant 1}\{\mu(dZ_{2n-1}\cap dS_1)-\mu(dZ_{2n}\cap dS_1)\}}. \quad (40)$$

Using Eq. (38), P_1 may be rewritten as

$$P_1=\frac{\sum_{n\geqslant 1}\{\mu(\Delta Z_{2n}\cap dS_1)+\mu(dZ_{2n-1}\cap dS_1)\}}{\sum_{n\geqslant 1}\{\mu(\Delta Z_n\cap dS_1)+2\,\mu(dZ_{2n-1}\cap dS_1)\}}. \quad (41)$$

It is clearly seen in Eq. (41) that $0\leqslant P_1\leqslant 1$.

D. Probabilities from a part of the entrance gate

It is also interesting to compute the probability of reaction of trajectories originating from a particular region of ΔU_1, where the dynamical variable Ω takes a value we are interested in. This region will be transported in the course of the reaction towards the exit gate. We shall thus calculate the reaction probability or the mean value of some observable, provided that we originate only from a particular part of the entrance gate, chararacterized, through the Hamiltonian flow from $\mathcal{S}^{\infty}$ to Σ, by some values of the observables. Let us call the region inside ΔU_1, ΔC_1.

On the regular part, we define

$$\Delta C_n=\hat{M}^n(\Delta C_1)\cap\Delta Z_n.$$

Once more, as in Sec. V C, the regular parts are calculable numerically: One measures thus the sucessive images ΔC_n of ΔC_1 and the areas of the intersections $(\Delta C_n\cap\Delta Z_n)\cap\Delta S_1$. For the regular parts, it is useless to introduce probabilities.

However, the statistical zones of ΔS_1 are described by two probabilities: P_n^0, the probability of finding a reactive trajectory in the ensemble $(\Delta Z_n\cap\Delta C_n)\cap\Delta S_1$, and P_n^z, the probability of finding inside some winding dZ_n a trajectory originating from ΔC_1. We need to know both P_n^0 and P_n^z in order to know the probability of a winding to contain an image of ΔC_1 that is odd, that is, a part of ΔC_1 that reacts. We again make the hypothesis that windings are uniformly distributed inside dZ_n, so that P_n^0 and P_n^z are uniform. Therefrom, for the same reasons as before [Eq. (35)], one has

$$P_n^0=\begin{cases}P_1^0 & \text{for odd } n\\ 1-P_1^0 & \text{for even } n.\end{cases} \quad (42)$$

Furthermore, taking into account that dZ_{n+1} is the image of dZ_n and windings are uniform in dZ_n, we have

$$P_n^z=P_1^z \quad \forall n. \quad (43)$$

In order to calculate P_1^z, we remember that the windings dZ_1 are coming from the intersections $\Delta Z_n\cap dS_1$ and $dZ_n\cap dS_1$. Thus

$$P_1^z\mu(dZ_1)=\sum_{n\geqslant 1}\mu(\Delta C_n\cap dS_1)+P_1^z\sum_{n\geqslant 1}\mu(dZ_n\cap dS_1). \quad (44)$$

Extracting P_1^z and recalling the definition of ΔZ_n, Eqs. (31) and (32), one obtains

$$P_1^z=\frac{\sum_{n\geqslant 1}\mu(\Delta C_n\cap dS_1)}{\sum_{n\geqslant 1}\mu(\Delta Z_n\cap dS_1)}. \quad (45)$$

Now, for P_1^0, the derivation is similar to that in Sec. V C, by inserting the appropriate P_1^z,

$$P_1^0P_1^z\mu(dZ_1)=\sum_{n\geqslant 1}\mu(\Delta C_{2n}\cap dS_1)+P_1^z\left[P_1^0\sum_{n\geqslant 1}\mu(dZ_{2n}\cap dS_1)+(1-P_1^0)\sum_{n\geqslant 1}\mu(dZ_{2n-1}\cap dS_1)\right]. \quad (46)$$

Therefrom, we deduce the probability of reaction, coming from the area ΔC_1:

$$P_1^0=\frac{\sum_{n\geqslant 1}\mu(\Delta C_{2n}\cap dS_1)+P_1^z\sum_{n\geqslant 1}\mu(dZ_{2n-1}\cap dS_1)}{P_1^z\left[\sum_{n\geqslant 1}\mu(\Delta Z_n\cap dS_1)+2\sum_{n\geqslant 1}\mu(dZ_{2n-1}\cap dS_1)\right]}. \quad (47)$$

Equations (41) and (47) are the main quantitative results of this paper. Together with the actual measuring of the intersections of surfaces, they allow for a prediction of a reaction rate or any observable, from the whole entrance gate or a suitable part of it.

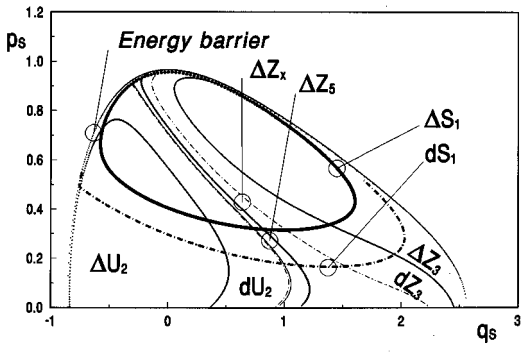

FIG. 14. Overall outcome of the reaction, with the parameters described in Sec. VI. The different zones that cover the exit gate $\Delta S_1 \cup dS_1$ are shown. The limits of the ΔU_n sets are in full lines and the limits of halos in dot-dashed lines. The numerical values of the areas are given in Table I.

VI. NUMERICAL RESULTS

In order to verify our previous analysis, it is interesting to illustrate it with a specific example. We keep the same parameters as before, namely, $\tilde{E}=1.4$ and $m_A/m_B=0.5$ [Eq. (12)]. The ΔU_1 surface is supposed to have a constant density of probability $\rho(q_S,p_S)=$const. To start, we measure the different relevant surfaces of Fig. 14. Results are shown in Table I. Indeed, one sees that the number of $\Delta U_n, dU_n$ needed is very small. 97% of the surface of the exit halo $\mathcal{H}S_1$ is taken into account just by measuring the intersections with $\Delta U_n, dU_n, n=1,\ldots,5$. Also, ΔZ_4 has no intersection, since [Fig. 9(c)] it lies totally in the $p_S<0$ region. A summary of the contributions to reaction rate is given in Table II. We also have to calculate P_1, the probability of being reactive inside an odd halo [Eq. (41)]. We find a value of $P_1=0.52$ showing that the halos are nearly equally divided into reactive and nonreactive trajectories. Also the relative importance of halos (nearly 40% of the total surface) is consistant with the large amount of chaos found in our earlier analysis; see [4]. There, it was found that the average number of loops, or successive maps in our present language, amounts to 5 at $\tilde{E}=1.4$. As only $\Delta Z_2, \Delta Z_3$ contribute significantly as nonwound regions to the reaction, it is clear that the larger number of loops comes from the halos dZ_2, dZ_3. The overall reaction rate is found at 58.7%. It is difficult at this stage to have an estimate of the error, which depends on many factors, uncontrolled at the moment. So the best comparison is with a well-established method, the sum-over-trajectory method. The maximum allowed incoming momentum at $\tilde{E}=1.4$ is [Eqs. (12) and (17)] $p_{1\,\max}=0.67$. By setting the appropriate weight function to account for $\rho=$const and by averaging over 1000 trajectories for each of the 13 momenta chosen, an overall mean reaction rate of 56.7% is found, in excellent agreement with the surface calculations. These results are summarized in Table II. It is clear that this comparison is for illustrative purposes for the moment. A series of calculations, with different sets of parameters, should show the influence of phase-space geometries on the rate of reaction and how good the halo-gateway method is with respect to a sum over trajectories.

TABLE I. Weights of the different intersections in Fig. 14. The notations refer to the figure. The parameters are $\tilde{E}=1.4$ and $m_A/m_B=0.5$.

Intersection	Weight (%)
$\Delta U_2 \cap \Delta S_1$	11.3
$\Delta U_2 \cap dS_1$	10.8
$dU_2 \cap \Delta S_1$	11.5
$dU_2 \cap dS_1$	4.0
$\Delta U_3 \cap \Delta S_1$	29.2
$\Delta U_3 \cap dS_1$	8.9
$dU_3 \cap \Delta S_1$	9.9
$dU_3 \cap dS_1$	5.8
$\Delta U_5 \cap \Delta S_1$	2.0
$\Delta U_5 \cap dS_1$	0.9
$dU_5 \cap \Delta S_1$	1.6
$dU_5 \cap dS_1$	0.5
remaining parts	3.6

TABLE II. Summary of the different contributions to the overall reaction rate.

	Weight (%)
P_1 [Eq. (41)]	52
direct (reactive)	42.0
halos (reactive)	16.7
Total reaction rate	
surfaces	58.7
trajectories	56.8

VII. DISCUSSION

The whole analysis we have proposed in this paper is based on a careful description of the motion at the asymptotic limit and on how this near-integrable motion projects itself onto the periodic orbit dividing surface Σ. Simply from that analysis, we have been able to reconstruct nearly the whole image of the chaos at hand. Indeed, it is because of the non-integrable nature of the Hamiltonian that any crossing of U_n and S_1 occurs at all [31,32]. For a nonchaotic Hamiltonian, S_1 and some U_n would coincide and the windings would disappear altogether. Any mixing would be absent in the course of the reaction. This simple reasoning shows also how particular the integrable case is.

In the course of the analysis, we have been able to define on the Σ surface two particular zones, which form together the gateway. This gateway may be crossed only once by any trajectory going to or leaving the interaction region. It is thus tempting to identify our gateway with a classical image of the transition state. It must be borne in mind, however, that such an easy definition of the gateway was made possible by the simplicity of the definition of the periodic orbit dividing surface Σ. It is not yet clear how to define a gateway in a direct reaction such as $H+H_2 \rightarrow H_2+H$, where at minimum distance there is a potential barrier instead of a well.

The extent of the intersections of the exit gate and the

successive maps of the entrance gate determines the overall shape of the reaction. If nearly all trajectories leave after a few mappings, the reaction will look simple from the outside and the intermediate product short lived. On the other hand, a domination of several high-order mappings will shift the balance towards complicated trajectories and a long-lived intermediate complex. However, one must recall that the *whole* motion in phase space is analyzed here in the framework of fully chaotic motion: hyperbolic motion in the surface of section Σ in the language of dynamics. This is what allowed us to speak about unstable periodic orbits and their stable and unstable manifolds that cross and wind. Otherwise stated, if for some defined value of n, $\Delta U_n \cap \Delta S_1$ is very large, most trajectories will exit after n loops. But the essence of the analysis shows that for some region of the entrance gate, a complex situation will indeed occur whose statistical weight is small.

It has often been observed that for some regions of the reaction parameters, the course of the scattering looks regular and for some other regions it looks chaotic [33]. One is then tempted to find a border between chaotic and nonchaotic zones in reaction processes. We feel that examination of the various intersections of the gateway mappings provides a quantitative and qualitative basis for this distinction. It properly underlines the necessary coexistence of long-lived and short-lived trajectories and the fuzziness of the barrier between chaotic and nonchaotic motion.

The gateway we defined is surrounded by a series of infinitely elongated images of itself, created by the Hamiltonian flow, as we described in detail: the windings. This is an image in the Poincaré section of both chaos and asymptotic integrability. It is clear that this image, characteristic of classical mechanics —infinitely detailed structure, hierarchically organized with a fractal set of discontinuities—cannot survive in the real physical world. In particular, the reaction we examine cannot survive a long time without being subjected to any concievable kind of external perturbation; also the spatial extent of the reaction must be short in order for the atoms not to be subjected to forces originating from outside. It is absolutely necessary to introduce time scales and length scales over which the full classical dynamics cannot survive. This has brought us to introduce the concept of halos. We believe that they should constitute a model of a bridge between rigorous classical mechanics and the real physical world in this context.

Halos are formed by the windings around the images of the entrance and exit gates. Since the dynamics inside the windings is infinitely complicated, we replace the exact picture by a statistical one. The border of a halo is determined by some physical or geometrical arguments and inside the halo, we have made the assumption of an equirepartition of the different levels of the hierarchy, each with its own overall probability. We are then able to calculate the relevant density probabilities inside the halos and proceed towards reaction rates or average of observables. We showed how precisely this method works, even when we include very large halos around the gateways and cut the hierarchy already at the fifth level, thereby avoiding all influence of the Kol'mogorov-Arnold-Moser region.

As we proceed deeper and deeper into the hierarchies of ΔU_n, we have seen that the relative importance of the regular, unwound parts diminishes with respect to the irregular parts, inside windings. In our case, as soon as $n \geqslant 7$, all levels become superficially alike, consisting of windings of windings around the main $\Delta U_1, \Delta U_2, \Delta Z_3$ sets. In that way, all high-order contributions to chaos are put inside the halos of some lower-order set. The halos *replace* the whole complicated structure that unfolds as we go into higher and higher n. We may thus say that halos cut the hierarchy at some level and allow us to simplify drastically the whole picture. It is thus in some defined part of the phase space, the ensemble of the halos, that the old statistical assumptions of equirepartition of reactants [34] gain some validity. It would be most interesting to compare the gateway-halo method to some pure statistics in the case of very extended chaos (small measure of the ΔZ_n ensembles).

As we have said earlier, once the trajectory leaves the interior of the interaction region, a sensible model should include the possibility of that trajectory being perturbed: When the diatom is far from the atom for a sufficiently long time, it experiences perturbations from the exterior world. The model used here is microcanonical, so that energy is conserved. Also, the perturbation acts only far from the center. Its effect is thus to move the representative point in phase space to another point in the same energy shell, also far from the interaction region. In the picture used here, the different windings that form the halos are blurred, leading to the statistical assumption inside the halos. Actually, it was not physically meaningful to suppose that a long-lived trajectory, extending far away, ''remembers'' where it came from, even if this memory is the condition for the hierarchic organization of chaos.

Also, this image of a gateway surrounded by its halos, living in phase space, is easily adaptable to a semiclassical framework in a time-dependent or -independent picture. Indeed, halos provide a natural way of smoothing structures with respect to some characteristic action S, to be compared to $\hbar$. In that sense, one may also say that halos are a classical image for the quantum resonances that are seen in triatomic collisions, when the outgoing diatomic fragment has much of its energy trapped in a high vibrational state [35].

As alluded to in the Introduction, several authors already began to decribe the structure of the periodic orbit dividing surface Σ. The cylindrical manifolds of DeLeon *et al.* [18] are quite similar to our U_1 and S_1. However, these authors did not consider scattering but closed the phase space and in subsequent works concentrated rather on isomerization processes. However, the structuring role of the stable or unstable manifolds of carefully chosen periodic orbits is clearly seen, as well as the importance of their first and last intersections with the Σ section, called reactive islands. However, the possibility of having finite area per infinite perimeter islands, while being latent in the figures, was not clearly described. The successive images of U_1 and S_1, which build up the phase-space image of the reaction [the R transformation, Eq. (23)], have been described in some detail, with some glimpses of the windings, by Pollak *et al.* [13,14], principally in the framework of the transition state theory. A general review is provided in Ref. [36]. The reaction rate has also been calculated either by minimizing and maximizing flux through sections (a TST approach) or by use of the maximum-entropy principle in the irregular regions of Σ.

Since scattering chaos was not yet fully understood as a dynamical system, there was no attempt to clearly circumscribe chaos in regions, the halos, where probabilities may be defined. However, a fully mixing dynamics was implicitly hypothesized in the windings, so that maximum entropy could be used. Another surface of section was used by Davis and co-workers [15–17], more or less along the reaction path (hyerbolic coordinates). They clearly understood that there was chaos in their system, very similar to ours. In light of the present work, their Figs. 11–17 [17] describe the successive images of U_1 and S_1, in a somewhat different context—three dividing periodic orbits at finite distance—but windings are not seen as such. However, the surface of section used need not represent faithfully the Hamiltonian flux, since it is not an attractive PODS, in the language of Pollak. Still, in Refs. [15,16], the gateway is clearly present and its importance properly stressed (e.g., Fig. 10, Ref. [15]). The appearance of successive intersections of the lobes of the unstable manifolds (U_n now) with the first lobe of the stable manifold (S_1 now) is also described and these intersections were rightfully incorporated into the reaction rate. In retrospect, the very importance of gateways and their images in phase space were apprehended already in the mid 1980s. Now, thanks to the firm theories on the existence and properties of scattering chaos, it has been possible to pursue further the analysis begun some time ago, towards a quantitative analysis.

The procedure we have proposed here has to be extended in three ways. First, one has to deal with realistic collinear processes, with inclusion of potential holes and hills, as well as a good asymptotic behavior (e.g., van der Waals). Second, and this is also not too demanding, we may include temperature in the formalism. The gateway will extend through a third dimension, energy, so that it still remains possible to visualize it. The halos should still surround it and some model of mixing in phase space plus energy is to be included. But the most important and demanding extension is towards three degrees of freedom, including rotation and vibration of the AB fragment. Poincaré sections are now four dimensional, difficult to visualize. However, the situation is not hopeless, thanks to the tremendous simplification of asymptotic separation of motions.

VIII. CONCLUSION

We have thus shown in this paper how to calculate reaction rate in the presence of classical chaos in a simple, yet meaningful, example. Rather than resorting to a blind averaging process, we have used a quantitative description of the geometrical motion in phase space. With the help of the definitions of the statistical zones, the halos, we have been able to get rid of the classical intricacies of chaos in a physically meaningful and numerically controlled fashion, thus opening the way to a geometrical analysis of simple chemical reactivity.

ACKNOWLEDGMENT

The authors wish to thank J. C. Rayez for encouraging and fruitful discussions.

APPENDIX A

Let us recall the notations of Sec. IV. From what we have said, the trajectory going through P will see its translational kinetic energy go to zero on $\mathcal{S}^{\varepsilon_0}$. The state of the system is then represented by a point on the curve Γ^{ε_0}. If we go along $\overline{PI}$, from P to I, following hypotheses (ii) and (iv), we define an ensemble of trajectories, all defined uniquely by the index ε. Let us denote $\mathbf{x}^{\varepsilon}(t)$ such a trajectory ($\mathbf{x}$ is a point in phase space). Each trajectory $\mathbf{x}^{\varepsilon}(t)$ crosses on a specific point M^{ε}, on the curve Γ^{ε}. On the section $\mathcal{S}^{\varepsilon_0}$, $\varepsilon_0>\varepsilon$, the trajectory $\mathbf{x}^{\varepsilon}(t)$ has two crossing points: on its way out $M_{-}^{\varepsilon,\varepsilon_0}$ and on its way back from $\mathcal{S}^{\varepsilon}$, $M_{+}^{\varepsilon,\varepsilon_0}\in\Gamma^{\varepsilon,\varepsilon_0}$. We note $t(\varepsilon,\varepsilon_0)$, the time the representative point takes to go back and forth, between $M_{-}^{\varepsilon,\varepsilon_0}$ and $M_{+}^{\varepsilon,\varepsilon_0}$. The trajectory $\mathbf{x}(\varepsilon,t)$ has enough translational energy to go to the section $\mathcal{S}^{\varepsilon}$, which is the farthest it can go. $\overline{v(\varepsilon)}$ is the average speed (in modulus) for such a trajectory $\mathbf{x}(\varepsilon,t)$, between section $\mathcal{S}^{\varepsilon_0}$ and $\mathcal{S}^{\varepsilon}$ (Fig. 7).

Lemma 1.

$$\lim_{\varepsilon\to 0}\overline{v(\varepsilon)}=0\,. \tag{A1}$$

Demonstration. Let us set the origin of times when $\mathbf{x}(\varepsilon,t)$ crosses $\mathcal{S}^{\varepsilon_0}$. So $\mathbf{x}(\varepsilon,0)\in\mathcal{S}^{\varepsilon_0}$ and $\dot{r}_{oi}>0$, so that $\mathbf{x}(\varepsilon,t(\varepsilon_0,\varepsilon_0))\in\mathcal{S}^{\varepsilon_0}$ and $\dot{r}_{oi}<0$. The discussion rests only on the period $0<t<t(\varepsilon_0,\varepsilon_0)$. During this period, (i) from the Hamiltonian equation, $\dot{r}_{oi}$ is a decreasing function of time, and (ii) the section $\mathcal{S}^{\varepsilon}$ recedes to infinity when $\varepsilon\to 0$ and the speed $\dot{r}_{oi}$ remains bounded so that $\lim_{\varepsilon\to 0}t(\varepsilon_0,\varepsilon)=\infty$. Let us choose an arbitrary speed $v>0$. We define on an $\mathbf{x}(\varepsilon,t)$ trajectory $t_{>}(\varepsilon,v)$, the amount of time during which $|\dot{r}_{oi}|>v$, and $t_{<}(\varepsilon,v)$, the amount of time during which $|\dot{r}_{oi}|<v$. Then

$$t_{>}(\varepsilon,v)\leqslant\sup_{\varepsilon\in\,]0,\varepsilon_0]}t_{>}(\varepsilon,v)<\infty,$$

so that

$$\lim_{\varepsilon\to 0}t_{<}(\varepsilon,v)=\infty.$$

Calling $v_{\max}$ the maximum of v on the trajectory, we have the inequalities

$$0\leqslant\overline{v(\varepsilon)}\leqslant\frac{t_{>}(\varepsilon,v)v_{\max}}{t_{>}(\varepsilon,v)+t_{<}(\varepsilon,v)}+\frac{t_{<}(\varepsilon,v)v}{t_{>}(\varepsilon,v)+t_{<}(\varepsilon,v)}, \tag{A2}$$

so that

$$0\leqslant\lim_{\varepsilon\to 0}\overline{v(\varepsilon)}\leqslant\lim_{\varepsilon\to 0}\left\{\frac{t_{>}(\varepsilon,v)v_{\max}}{t_{>}(\varepsilon,v)+t_{<}(\varepsilon,v)}+\frac{t_{<}(\varepsilon,v)v}{t_{>}(\varepsilon,v)+t_{<}(\varepsilon,v)}\right\} \tag{A3}$$

and

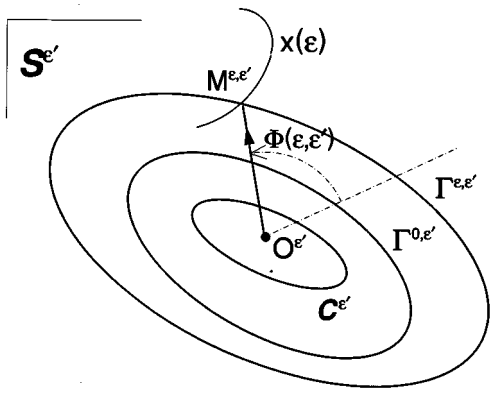

FIG. 15. Scheme for the theorem (Appendix C).

$$0 \leqslant \lim_{\varepsilon \to 0} \overline{v(\varepsilon)} \leqslant 0 + v. \tag{A4}$$

Equation (A4) being valid for any value of v, one has the desired result (A1).

APPENDIX B

The notations are the same as before. $t(\varepsilon_0,\varepsilon)$ is considered as a function of ε, $0<\varepsilon\leqslant\varepsilon_0$.

Lemma 2. $t(\varepsilon_0,\varepsilon)$ is a decreasing function of ε.

Demonstration. Let us denote by $d(\varepsilon)$ the distance separating section $\mathcal{S}^{\varepsilon_0}$ from $\mathcal{S}^{\varepsilon}$: $d(\varepsilon)=r_{oi}(\varepsilon)-r_{oi}(\varepsilon_0) = -\ln(\varepsilon/\varepsilon_0)$. We have $t(\varepsilon_0,\varepsilon)=d(\varepsilon)/\overline{v(\varepsilon)}$. Denoting by the prime the derivation with respect to ε, we have

$$t'(\varepsilon_0,\varepsilon)=\frac{d'(\varepsilon)\overline{v(\varepsilon)}-d(\varepsilon)\overline{v'}(\varepsilon)}{\overline{v^2}(\varepsilon)}.$$

Following Lemma 1, $\overline{v(\varepsilon)}\simeq\overline{v(0)}+\gamma\varepsilon=\gamma\varepsilon$. Then,

$$t'(\varepsilon_0,\varepsilon)=\frac{-1+\ln(\varepsilon/\varepsilon_0)}{\gamma\varepsilon^2}+\cdots. \tag{B1}$$

Since $\overline{v(\varepsilon)}>0$, $\gamma>0$; consequently $t'(\varepsilon_0,\varepsilon)<0$ for ε sufficiently small.

APPENDIX C

Following from the theorem of Sec. IV B, we have the following.

Demonstration. Let $\{\mathcal{C}^{\varepsilon};\varepsilon\in]0,\varepsilon^0]\}$ be a familiy of closed convex curves with the following properties (see Fig. 15).

(i) $\mathcal{C}^{\varepsilon}\in\mathcal{S}^{\varepsilon}\forall\varepsilon\in]0,\varepsilon^0]$.

(ii) $\mathcal{C}^{\varepsilon}$ is inside $\Gamma^{\varepsilon,\varepsilon'}$, for any couple $0<\varepsilon'\leqslant\varepsilon\leqslant\varepsilon_0$.

(iii) The projection of the $\mathcal{C}^{\varepsilon}$ curves onto the (r_{o2},p_{o2}) space does not depend on ε. Otherwise stated, the equation $\mathcal{C}^{\varepsilon}(r_{o2},p_{o2})=0$ that defines the curve $\mathcal{C}^{\varepsilon}$ on $\mathcal{S}^{\varepsilon}$ does not depend explicitly on ε.

That one can construct such a family of curves is obvious. Now, for each curve $\mathcal{C}^{\varepsilon}$, we associate a point O^{ε}, defined by some (r_{o2},p_{o2}) coordinates not depending on ε. O^{ε} is inside the $\mathcal{C}^{\varepsilon}$ curves. Let us now consider one of those families $\{\mathcal{C}^{\varepsilon};O^{\varepsilon};\varepsilon\in]0,\varepsilon^0]\}$. We shall now parametrize each curve by a phase Φ, in the following way: The value of Φ on $\mathcal{C}^{\varepsilon}$ is defined mod 2π and the same phase is associated with two points $(r_{o2},p_{o2},\varepsilon)$ and $(r_{o2},p_{o2},\varepsilon')$, which differ only by the section $\mathcal{S}$ to which they belong (i.e., by the fact that $\varepsilon\neq\varepsilon'$). Let us recall that the trajectory denoted by $\mathbf{x}(\varepsilon,t)$ has enough translational energy to go up to the section $\mathcal{S}^{\varepsilon}$. We associate now a phase $\Phi(\varepsilon,\varepsilon')$ with that trajectory in the following way. At time t, the trajectory $\mathbf{x}(\varepsilon,t)$ reaches the section $\mathcal{S}^{\varepsilon'}$, on the point $M^{\varepsilon,\varepsilon'}=\mathbf{x}(\varepsilon,t)\cap\mathcal{S}^{\varepsilon'}$. We define the phase by the oriented segment $[O^{\varepsilon'},M^{\varepsilon,\varepsilon'}]$; see Fig. 15.

Now that a phase is associated with a trajectory in the asymptotic domain, the demonstration proceeds in two stages. In the first stage the winding theorem is valid on $\mathcal{S}^{\varepsilon_0}$, that is, if M^{0,ε_0} belongs to Γ^{0,ε_0}, if the $\overline{M^{\varepsilon_0,\varepsilon_0}M^{0,\varepsilon_0}}$ segment is of finite length when $p_{o1}>0$ (outgoing trajectory), and there exists a bijection between $\overline{M^{\varepsilon_0,\varepsilon_0}M^{0,\varepsilon_0}}$ and the interval $[\varepsilon_0,0]$, then $\overline{M^{\varepsilon_0,\varepsilon_0}M^{0,\varepsilon_0}}$, $p_{o1}<0$ (incoming trajectory) is a spiral curve winding infinitely around Γ^{0,ε_0}. In the second stage, if the theorem is true on $\mathcal{S}^{\varepsilon_0}$, it is true on Σ.

To demonstrate the first stage, let us denote by $\Phi^I(\varepsilon)$ the phase of the trajectory $\mathbf{x}(\varepsilon,t)$ on the first crossing of $\mathcal{S}^{\varepsilon_0}$ (outgoing, $p_{o1}>0$) and $\Phi^F(\varepsilon)$ the phase of the trajectory $\mathbf{x}(\varepsilon,t)$ on the second crossing of $\mathcal{S}^{\varepsilon_0}$ (ingoing, $p_{o1}<0$). We define a time $\tau(\varepsilon)$ as

$$\Phi^F(\varepsilon)-\Phi^I(\varepsilon)=\frac{2\pi}{\tau(\varepsilon)}t(\varepsilon_0,\varepsilon), \tag{C1}$$

where $2\pi/\tau(\varepsilon)$ represents the average phase velocity for the trajectory $\mathbf{x}(\varepsilon,t)$ between its two crossings of $\mathcal{S}^{\varepsilon_0}$. Let us examine Eq. (C1) for $\varepsilon\to0$. We have the following.

(i)

$$\tau(\varepsilon)=\tau(0)+\theta_1(\varepsilon),$$

where

$$\lim_{\varepsilon\to0}\theta_1(\varepsilon)=0.$$

Indeed, when $\varepsilon\to0$, the trajectory spends an arbitrary long time arbitrarily near the section at infinity $\mathcal{S}^0$. Now, near $\mathcal{S}^0$, trajectories tend to follow arbitrarily closely the evolution of a Morse oscillator of energy $E-1$. Then, time $\tau(\varepsilon)$ converges towards a value $\tau(0)\neq0$, so that

$$\frac{2\pi}{\tau(\varepsilon)}=\frac{2\pi}{\tau(0)}[1+\theta_2(\varepsilon)].$$

where, as in the previous case,

$$\lim_{\varepsilon\to0}\theta_2(\varepsilon)=0.$$

(ii) The segment $\overline{M^{\varepsilon_0,\varepsilon_0}M^{0,\varepsilon_0}}$ is of finite length. Indeed, it is the image by the Hamiltonian flux of a finite length segment $\overline{PI}$ over a finite time. As $\overline{PI}$ is parametrized by a continuous index, it is always possible to write

$$\Phi^I(\varepsilon)=\Phi^I(0)+\theta_3(\varepsilon),$$

again with

$$\lim_{\varepsilon\to 0}\theta_3(\varepsilon)=0.$$

Summarizing, we write the result

$$\Phi^F(\varepsilon)=\phi^I(0)+\frac{2\pi}{\tau(0)}t(\varepsilon_0,\varepsilon)+\theta(\varepsilon),$$
$$\lim_{\varepsilon\to 0}\theta(\varepsilon)=0. \tag{C2}$$

Equation (C2) means that $\Phi^F(\varepsilon)$ behaves like $t(\varepsilon_0,\varepsilon)/\tau(0)$. Following the sign of $\tau(0)$, for sufficiently small values of ε, the function $\Phi^F(\varepsilon)$ is a decreasing (increasing) function of ε, going to $+\infty$ $(-\infty)$ when ε goes to zero.

To demonstrate the second stage let us consider, on Fig. 15, with $\varepsilon'=\varepsilon_0$, the oriented segment $\overline{O^{\varepsilon_0}M^{\varepsilon,\varepsilon_0}}$. This segment has, by the Hamiltonian flux, an image on Σ of finite length, extending away from U_1. The curve $\overline{M^{\varepsilon_0,\varepsilon_0}M^{0,\varepsilon_0}}$ cuts the $\overline{O^{\varepsilon_0}M^{\varepsilon,\varepsilon_0}}$ segment an infinite number of times, always in the same sense. Therefrom we deduce that $\hat{M}(\overline{PI})$ cuts an infinite number of times, always in the same sense, any oriented segment between U_1 and $U_1^{\varepsilon_0}$. We say that $\hat{M}(\overline{PI})$ winds around U_1. This concludes the demonstration.

[1] T. Tél, in *Directions in Chaos*, edited by Hao Bai-Lin (World Scientific, Singapore, 1993), Vol 3, p. 149.

[2] J.I. Steinfeld, J.S. Fransisco and W.L. Hase, *Chemical Kinetics and Dynamics* (Prentice-Hall, Englewood Cliffs, NJ, 1989).

[3] R.D. Levine and R.B. Bernstein, *Molecular Reaction Dynamics and Chemical Reactivity* (Oxford University Press, Oxford, 1987).

[4] Z. Kovács and L. Wiesenfeld, Phys. Rev. E **51**, 5476 (1995).

[5] R.S. MacKay, J.D. Meiss, and I.C. Percival, Physica D **13**, 55 (1984).

[6] S. Wiggins, *Chaotic Transport in Dynamical Systems* (Springer-Verlag, New York, 1992).

[7] O. Bohigas, S. Tomsovic, and D. Ullmo, Phys. Rep. **223**, 43 (1993).

[8] P. Brumer, Phys. Scr. **40**, 394 (1989), and references cited therein.

[9] U. Smilansky, in *Chaos and Quantum Physics*, 1989 Les Houches Lectures, Session LII, edited by M.J. Giaonnoni, A. Voros, and J. Zinn-Justin (North-Holland, Amsterdam, 1991), p. 371.

[10] B. Eckhardt, J. Phys. A **20**, 5971 (1987); E. Ott and T. Tél, Chaos **3**, 417 (1993).

[11] G.G. Balint-Kurti, F. Gögtas, S.P. Mort, and A.R. Offer (unpublished); A. Lagan and O. Gervasi, J. Chem. Phys. **99**, 9567 (1993).

[12] J. Manz and J. Römelt, J. Chem. Soc. Faraday Trans. **86**, 1689 (1990).

[13] P. Pechukas and E. Pollak, J. Chem. Phys. **71**, 2062 (1979); E. Pollak, M.S. Child, and P. Pechukas, *ibid.* **72**, 1669 (1980); M.S. Child and E. Pollak, *ibid.* **73**, 4365 (1980).

[14] E. Pollak and M.S. Child, J. Chem. Phys. **73**, 4373 (1980).

[15] M.J. Davis and S.K. Gray, J. Chem. Phys. **84**, 5389 (1986).

[16] M.J. Davis, J. Chem. Phys. **86**, 3978 (1987).

[17] R.T. Skodje and M.J. Davis, J. Chem. Phys. **88**, 2429 (1988).

[18] N. DeLeon, M.A. Mehta, and R.Q. Topper, J. Chem. Phys. **94**, 8310 (1991); **94**, 8329 (1991); N. DeLeon and S. Ling, *ibid.* **101**, 4790 (1994).

[19] I. Burghardt and P. Gaspard, J. Chem. Phys. **100**, 6395 (1994).

[20] M. Berblinger and C. Schlier, Chem. Phys. Lett. **145** 299 (1988).

[21] I. Burghardt and P. Gaspard, J. Phys. Chem. **99**, 2732 (1995).

[22] A. Tiyapan and C. Jaffé, J. Chem. Phys. **99**, 2765 (1993); **103**, 5499 (1995).

[23] V. Balasubramanian, B.K. Mishra, A. Bahel, S. Kumar, and N. Sathyamurthy, J. Chem. Phys. **95**, 4160 (1991).

[24] H. Wadi and L. Wiesenfeld, C. R. Acad. Sci. Paris Ser. II **322**, 621 (1996).

[25] E.J. Heller, J. Chem. Phys. **92**, 1718 (1990).

[26] M.A. Eliason and J.O. Hirshfelder, J. Chem. Phys. **30**, 1426 (1959).

[27] F.T. Smith, J. Chem. Phys. **31**, 1352 (1959).

[28] If we were to look into the other channel, we should have $r_{l2}\gg r_{l1}$, $r_e\Rightarrow q_2$ and $q_1\gg\widetilde{R}_e$, but $q_1-q_2\cot\varphi\sim\widetilde{R}_e$.

[29] Let us recall that here we neglect completely the nonhyperbolicity of the chaotic scattering process. Otherwise, it is clear that any of our statements about tiling is true only if we include somehow the stable elliptic islands, whose dynamics are disjoint from the scattering process. However, measures would still be conserved.

[30] In Ref. [22], the authors noted exactly this phenomenon; see their Fig. 2.

[31] A.J. Lichtenberg and M.A. Lieberman, *Regular and Stochastic Motion* (Springer-Verlag, New York, 1983).

[32] A.M. Ozorio de Almeida, *Hamiltonian Systems: Chaos and Quantization* (Cambridge University Press, Cambridge, 1988).

[33] L. Bonnet, J.C. Rayez, and Ph. Halvick, J. Chem. Phys. **99**, 1771 (1993).

[34] J.C. Light, J. Chem. Phys. **40**, 3221 (1964).

[35] H.J. Werner, C. Bauer, P. Rosmus, H.K. Keller, M. Stumpf, and R. Schinke, J. Chem. Phys. **102**, 3593 (1995).

[36] E. Pollak, in *Theory of Chemical Reaction Dynamics*, edited by M. Baer (CRC, Boca Raton, FL, 1988), p. 123.